THE JOURNAL OF PHYSICAL CHEMISTRY B

ARTICLE

pubs.acs.org/JPCB

Formation of Supported Lipid Bilayers at Surfaces with Controlled Curvatures: Influence of Lipid Charge

Maria Sundh,[†] Sofia Svedhem,[‡] and Duncan S. Sutherland*[,†]

[†]Interdisciplinary Nanoscience Center (iNANO), University of Aarhus, 8000 Aarhus, Denmark

[‡]Department of Applied Physics, Chalmers University of Technology, 412 96 Gothenburg, Sweden

ABSTRACT: We have developed and characterized novel biomimetic membranes, formed at nanostructured sensor substrates with controlled curvatures, motivated by the many biological processes that involve membrane curvature. Model systems with convex nanostructures, with radii of curvatures (ROCs) of 70, 75, and 95 nm, were fabricated utilizing colloidal assembly and used as substrates for supported lipid bilayers (SLBs). The SLBs were formed via vesicle adsorption and rupture, and the vesicle deposition pathway was studied by means of quartz crystal microbalance with dissipation (QCM-D) and fluorescence microscopy. SLBs conforming to the underlying nanostructured surfaces, which exhibit increased surface area with decreased ROC, were confirmed from excess mass, monitored by QCM-D, and excess total fluorescence intensities. The formation of SLBs at the nanostructured surfaces was possible, however, depending on the ROC of the structures and the lipid vesicle charge the quality varied. The presence of nanostructures was shown to impair vesicle rupture and SLB formation was progressively hindered at surfaces with structures of decreasing ROCs. The introduction of a fraction of the positively charged lipid POEPC in the lipid vesicle membrane allowed for good quality and conformal bilayers at all surfaces. Alternatively, for vesicles formed from lipid mixtures with a fraction of the negatively charged lipid POPS, SLB formation was not at all possible at surfaces with the lowest ROC. Interestingly, the vesicle adsorption rate and the SLB formation were faster at surfaces with nanostructures of progressively smaller ROCs at high ratios of POPS in the vesicles. Development of templated SLBs with controlled curvatures provides a new experimental platform, especially at the nanoscale, at which membrane events such as lipid sorting, phase separation, and protein binding can be studied.

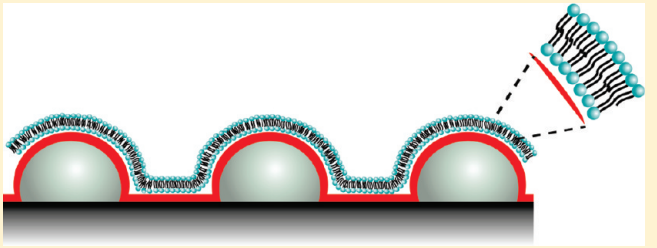

INTRODUCTION

Cell membranes are self-assembled supramolecular structures, which function as biological compartmentalizers but are also essential units for life sustaining processes occurring at or within the membrane. The large variety of lipids and lipid conjugates, with different charge, melting temperature, and shape, in the cell membrane allows for local accommodation to external stimuli by changing, e.g., its rigidity, fluidity, and curvature. A range of cellular processes involve bending of the lipid membrane to generate specific membrane structures, e.g., during the formation of filopodia and lamellopodia (upon cell migration),[1] vesicle trafficking,[2] and cell division.[3] The numerous cellular processes that involve curvature changes within the lipid membrane have led to the notion that curvature changes are not only passive consequences of cellular activity, but rather curvature itself provides a means for spatial organization of membrane constituents. In order to study curved lipid membranes and their influence on lipid sorting, phase separation, and preferential binding of proteins, a number of biomimetic systems, mimicking the natural cell membrane, have been developed. These include e.g. vesicles[4−6] and supported lipid bilayers (SLBs) on patterned solid substrates fabricated by optical lithography[7,8] and self-assembly of particles.[9,10] The approach of templating lipid membranes onto nanostructured surfaces has the advantage that the curvature of the nanostructures can be readily controlled during surface fabrication, giving the potential to define the curvature of an interacting membrane. In addition, it allows for the study of curvature related processes by means of surface sensitive techniques such as quartz crystal microbalance with dissipation (QCM-D) and atomic force microscopy.

Formation of SLBs via vesicle rupture, pioneered by McConnell et al.,[11] is a fast and reproducible approach to generate large areas of lipid bilayer membrane. The route of vesicle adsorption and subsequent SLB formation upon the deposition of vesicles on to a solid support has been shown to be dependent on parameters such as chemical[12,13] and structural[13,14] properties of the support, type of lipids used,[15,16] pH,[17] temperature,[17,18] and ionic strength[17] or osmotic pressure.[19] Even though many details of vesicle rupture have been revealed the process is still not completely understood. Three main vesicle deposition pathways have been identified; (i) vesicles adsorb and rupture directly or with the need for only few neighboring vesicles, (ii) vesicles adsorb and at a critical coverage of vesicles at the surface enough stress is exerted on the vesicles for the rupture process to start, and (iii) vesicles adsorb and stay intact. In addition, a fourth situation can occur where vesicles do not adsorb to the surface.

Received: March 17, 2011
Published: June 01, 2011

There is a broad range of lipids of interest for scientific or technical research and the choice of lipid or lipid mixture is dependent on the aim or application of each particular study. Negatively charged lipids are recognized by a number of membrane proteins with positively charged binding residues, examples include many of the proteins in the phospholipase A_2 family that catalyze the hydrolysis of ester bonds in phospholipids[20] and proteins containing BAR domains (Bin/Amphiphysin/Rvs domain), e.g., endophilin,[21] which binds and tubulates membranes. Positively charged lipids, although not naturally occurring, have been widely studied as a result of their potential for applications in drug and DNA delivery.[22]

This study aims at understanding the process of lipid vesicle adsorption and rupture at nanostructured templates, allowing for the fabrication of SLBs composed of biologically relevant lipids with controlled curvatures. The self-assembly based colloidal lithography approach is a fast and reproducible method to fabricate large areas of nanopatterns. Here, an extension of the colloidal lithography approach has been used where the nanoparticles have been heat treated to form convex structures with different but controlled radii of curvatures (ROCs) in a biologically relevant size range.[6,23] The adsorption of vesicles, which were in the same size regime as the nanostructures, and subsequent vesicle rupture was studied by means of QCM-D, and the quality of the final lipid bilayer was verified by QCM-D and fluorescence microscopy. The process of the rupture event of vesicles into SLBs on flat SiO_2 surfaces has been extensively studied using phosphocholine (PC) lipids by means of QCM-D.[16,19,24] The influence on the SLB formation process of positively and negatively charged lipids has mainly been investigated at flat surfaces and systematic studies have been performed with mixtures of DOPC and the positively charged lipid 1,2-dioleoyl-3-trimethylammonium propane (DOTAP, a non-phospholipid)[25] or the negatively charged lipid 1,2-dioleoyl-*sn*-glycero-3-phospho-L-serine (DOPS)[25−28] respectively. Experiments on a single composition of 1-palmitoyl-2-oleoyl-*sn*-glycero-3-phospho-L-serine (POPS) and 1-palmitoyl-2-oleoyl-*sn*-glycero-3-phosphocholine (POPC) have been performed with the purpose to study SLB formation at indium tin oxide.[29] On silicon dioxide, POPS and 1-palmitoyl-2-oleoyl-*sn*-glycero-3-ethylphosphocholine (POEPC) have been used to investigate lipid exchange between oppositely charged membranes.[30] In this work, the influence of the positively charged lipid POEPC and the negatively charged lipid POPS in mixtures with POPC was systematically studied; first on flat surfaces followed by nanostructured surfaces with controlled curvatures.

MATERIALS AND METHODS

All water was filtered and deionized using a Milli-Q plus purification unit (Millipore, France). 1-palmitoyl-2-oleoyl-*sn*-glycero-3-phosphocholine (POPC), 1-palmitoyl-2-oleoyl-*sn*-glycero-3-ethylphosphocholine (POEPC), 1-palmitoyl-2-oleoyl-*sn*-glycero-3-phospho-L-serine (POPS) were from Avanti Polar Lipids (AL, USA) and 1-palmitoyl-2-[6-[(7-nitro-2,1,3-benzoxadiazol-4-yl)amino]hexanoyl]-*sn*-glycero-3-phosphocholine (NBD-HPPC) from Invitrogen (USA). Buffer (10 mM tris(hydroxymethyl)-aminomethane (Tris) and 100 mM NaCl) was adjusted to pH 8.0 with HCl, and was filtered and degassed before use, sometimes with added ethylenediaminetetraacetic acid (EDTA) or $CaCl_2$. Ten mM sodium dodecyl sulfate (SDS) solutions were used for cleaning. AT-cut Au-coated QCM crystals, 5 MHz, were obtained from Q-Sense AB (Sweden). Polyelectrolytes used were poly(diallyldimethylammonium chloride) (PDDA, MW 200 000−350 000, Aldrich), poly(sodium 4-styrenesufonate) (PSS, MW 70 000, Aldrich), and polyaluminium chloride (PAX, Kemira Kemwater, Denmark). Polystyrene particles (sulfate latex 110 nm) were from Invitrogen (USA).

Vesicle Preparation. Lipid vesicles were formed by the extrusion method. In brief, the lipids were dissolved in chloroform at the desired ratio in wt % (for fluorescently doped vesicles 2% NBD-HPPC was added) in a round-bottom flask. The chloroform was evaporated under nitrogen gas during rotation of the flask to form a thin lipid film on the wall of the flask. Residual chloroform was evaporated under vacuum overnight. The lipid film was rehydrated in Tris buffer during repeated vortexing of the flask to form multilamellar vesicles. In some cases, 2 mM EDTA or $CaCl_2$ was added to the buffer. Unilamellar vesicles were formed by extrusion (2×11 times) through 100 nm filters (Avanti Polar Lipids, USA). The vesicles were stored under nitrogen gas at 4°C and used within 3−5 days. Vesicles were characterized in terms of sizes and zeta potentials using dynamic light scattering (Malvern Zetasizer Nano ZS, Malvern Instruments, U.K.) for POPC, POEPC, 10% POPS in the presence of 2 mM EDTA or $CaCl_2$. Vesicles had a size and a zeta potential of 155 ± 4 nm and −2.0 mV for POPC, 140 ± 6 nm and 44 mV for POEPC, 142 ± 3 nm and −15 mV for 10% POPS with EDTA, and 168 ± 1 nm and −6.0 mV for POPS with $CaCl_2$, respectively.

Surface Fabrication and Characterization. Silicon wafers and Au-coated QCM crystals (Q-sense, Sweden) were cleaned by sonication for 15 min each in acetone, ethanol, and water, followed by blowing dry with nitrogen gas. The substrates were further cleaned in UV/ozone for 1 h to remove organic carbon contamination, rinsed with water and blow dried. A monolayer mask of colloidal particles was electrostatically self-assembled by a process previously reported.[31] Here, a triple layer of polyelectrolytes were deposited on the substrates to give a positive charge at neutral pH. A sequential deposition was made of first 2% PDDA (by weight) in water for 30 s followed by a water rinse and blow drying, and then each of 2% PSS (by weight) and 5% PAX (by weight) were deposited in a similar manner. Negatively charged polystyrene particles (0.2% by weight in water) were allowed to adsorb to the positively charged surface for 2 min after which the substrates were rinsed with water and blow dried. For the fabrication of nanostructured substrates with different curvatures the substrates were subsequently heat treated at 110, 114, or 118 °C in air. Lastly, the substrates were sputter coated with a 4 nm titanium adhesion layer followed by 30 nm of silicon dioxide.

Substrates can be micro and macro patterned with nanostructures via controlled tape stripping.[32] In this study, on some of the samples, the particles were removed from half of the surface by tape stripping with a polydimethylsiloxane (PDMS) stamp prior to heat treatment and sputter coating with SiO_2. To determine the ROC of the particles, SEM images were taken at a 90° angle on cross sections of a minimum of 30 particles. From the SEM images a characteristic ROC was estimated by approximating the heated particles with a sphere embedded in the surface. Retrieving the particle heights from AFM imaging instead of SEM images resulted in no significant difference.

QCM-D. The main experimental technique used was QCM-D which is a surface sensitive technique that is able to detect adsorption and desorption of mass, in the ng/cm^2 range, to or from the surface of a quartz crystal sensor. The technique makes use of the piezoelectric property of quartz crystals, i.e., the crystal

mechanically deforms and starts to oscillate when it is subjected to an electric ac field. The resonance frequency at which the crystal is oscillating is dependent on the total oscillating mass and hence, any adsorbed or desorbed mass to or from the sensor surface will result in a frequency shift. For thin, rigid, films such as SLBs there is a linear relationship between the change in frequency and the adsorbed mass.[24] In addition to mass, viscoelastic and structural changes of the adsorbed material can be monitored through simultaneous dissipation measurements. Depending on the properties of the adsorbed film as well as of the surrounding media the energy stored in the oscillation will be lost, i.e. dissipate to heat, at different rates. Vesicle rupture and SLB formation was studied using a QCM E4 equipment (Q-Sense AB, Sweden). Before measurements the QCM crystals were soaked in an SDS solution overnight, rinsed with water, blow dried, and cleaned in UV/ozone for 40 min. Measurements were performed on four crystals with different curvatures (70, 75, and 95 nm ROC and flat) in parallel at a flow of buffer of 0.2 mL min^{-1} and at a temperature of 22 °C. At a stable baseline, the buffer was exchanged with vesicle solution (0.2 mg mL^{-1}) and vesicle adsorption was studied. For measurements carried out with positively charged lipids the vesicle solution was allowed to flow through the chambers for 5 min and was exchanged with buffer at t = 10 min. For all measurements carried out with negatively charged lipids, except 20% POPS in the presence of EDTA, vesicles were allowed to flow through the chambers for 5 min, at t = 10 min the pump was stopped, and at t = 20 min the flow was restarted and the vesicle solution was exchanged for buffer. For measurements with vesicles composed of 20% POPS in the presence of EDTA the pump was stopped at t = 10 min and left overnight to reach a stable end point and the QCM chambers were then rinsed with buffer. Frequency and dissipation shifts were monitored at the seventh overtone and have been normalized to the fundamental frequency. Four experiments were conducted for each curvature and lipid composition.

Fluorescence Microscopy. Fluorescence microscopy was used to study the fluidity of the membranes on SiO_2 coated flat and nanostructured QCM crystals and the total fluorescence intensities were studied on silicon wafers cleaned and fabricated as above. The measurements were performed on a Zeiss Axioplan 2E MOT microscope with a 40× water immersion objective and pictures were taken with an Axiocam camera. Compositions studied were POPC, POEPC, and 10% POPS in EDTA containing buffer and calcium containing buffer at all curved surfaces. Experiments were performed in batch mode at room temperature with a lipid vesicle concentration of 0.2 mg mL^{-1}. Fluorescence recovery after photobleaching (FRAP) was performed by bleaching a small spot (~35 μm) of the lipid layer adsorbed at the surface with a Hg lamp for 10 s after which the lipid layer was left to recover. Pictures were taken 0, 1, 3, and 5 min after bleaching.

RESULTS

The possibilities of, in real time, monitoring vesicle adsorption and subsequent vesicle rupture, on solid surfaces through changes in the acoustically coupled mass and the viscoelastic properties of a lipid layer on a sensor surface, make the QCM-D an outstanding technique for the study of vesicle deposition pathways and SLB formation. The ability of the QCM-D to distinguish between adsorbed bilayer patches and adsorbed intact vesicles has resulted in the formulation of two distinctly different mechanisms for SLB formation, i.e., via direct vesicle rupture or via a critical coverage pathway. Representative final values for SLBs formed at 5 MHz sensor crystals are $\Delta f \sim -26$ Hz (normalized to the fundamental frequency) and $\Delta D < 0.5 \times 10^{-6}$, respectively.[24] These are characteristic values for a rigid lipid layer on the sensor surface which corresponds to ~460 ng/cm^2 (as modeled by the Sauerbrey relation).[24]

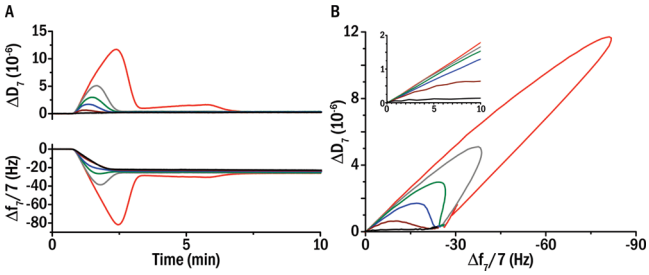

Figure 1. (A) Typical QCM-D results showing the dissipation and frequency shifts during the adsorption process of vesicles composed of POPC (red) and POPC doped with 20% (gray), 40% (green), 60% (blue), 80% (brown), and 100% (black) POEPC. Vesicles are deposited at 1 min and the surfaces are rinsed with buffer at 6 min. (B) A *Df*-plot with the same data as shown in part A but plotted as dissipation shift vs frequency shift. The inset shows the initial 10 Hz of the *Df*-plot.

Vesicle Adsorption and SLB Formation at Flat Surfaces. The results generated from QCM-D measurements at flat SiO_2 surfaces will be presented in terms of the influence of (i) positively charged lipids and (ii) negatively charged lipids in the lipid vesicles and the consequences observed in the vesicle deposition pathway, i.e. SLB formation via direct vesicle rupture or SLB formation via a critical vesicle coverage.

(i) Figure 1 shows the dissipation and frequency shifts occurring during the interaction of lipid vesicles composed of different percentages of POEPC and POPC with flat SiO_2 surfaces. Deposition of vesicles composed of purely the positively charged lipid POEPC, resulted in dissipation shifts which increased and frequency shifts which decreased monotonously (see black curve in Figure 1A) to values which are expected for good quality SLBs (here 23.9 ± 1.0 Hz and 0.3 ± 0.2 × 10^{-6}, Table 1). This indicates that vesicle rupture occurs directly upon vesicle adsorption, or alternatively with only the need for a few neighboring vesicles, which is in agreement with what has previously been shown by, e.g., Richter et al.,[25] using mixtures of DOPC and DOTAP, and by Edvardsson et al.,[33] using POEPC.

There are characteristic features in the QCM-D signals for SLB formation following vesicle crowding on the surface in the form of extrema in both the dissipation and frequency responses. There is a dip in the frequency response as a result of increased mass coupled to the oscillation of the crystal as vesicles adsorb, followed by mass loss when vesicles rupture and water coupled inside the vesicles is released. Similarly, the higher rigidity of the surface before vesicle adsorption as well as of the formed SLB compared to adsorbed intact vesicles gives rise to a transient peak in the dissipation shift. Upon decreasing the proportion of POEPC, by introducing POPC in the lipid vesicles, the vesicle deposition pathway changed to one with a need for a critical coverage of vesicles (Figure 1 and Table 1). Already at the introduction of low proportions of POPC, the resulting QCM-D graphs showed extrema in

Table 1. Mean Values and Corresponding Standard Deviations of Parameters Measured by QCM-D upon the Deposition of POPC Vesicles, with Varying Percentages of POEPC, to a Silicon Dioxide Surface

POEPC (%)	$\lvert\Delta f_{7,\min}\rvert/7$ (Hz)	$\lvert\Delta D_{7,\max}\rvert$ (10^{-6})	$\Delta f_{7,\text{final}}/7$ (Hz)	$\Delta D_{7,\text{final}}$ (10^{-6})	$t_{\min}$ (min)
0	91.4 ± 14	13.1 ± 1.9	−26.5 ± 0.7	0.53 ± 0.3	1.8 ± 0.3
20	40.0 ± 1.6	5.33 ± 0.3	−26.7 ± 0.4	0.65 ± 0.1	1.1 ± 0.0
40	26.2 ± 0.6	2.89 ± 0.1	−26.3 ± 0.7	0.53 ± 0.3	1.0 ± 0.0
60	-	1.68 ± 0.2	−25.2 ± 0.3	0.32 ± 0.0	-
80	-	0.61 ± 0.1	−25.2 ± 0.9	0.47 ± 0.3	-
100	-	-	−23.9 ± 1.0	0.33 ± 0.2	-

the dissipation shifts while the frequency shifts decreased monotonously. This indicates that the presence of the zwitterionic lipid POPC reduces the vesicle-surface interaction and that the vesicles need additional stress, albeit small, in the form of neighboring vesicles in order to rupture. A further increase in the proportion of POPC to ~60% (40% POEPC) resulted in the presence of extrema in both the dissipation and the frequency responses. The peak amplitudes increased with decreasing proportions of POEPC, indicating the need for increased critical coverage of vesicles for the rupture process to start. At the extrema there are more vesicles rupturing into SLB, and releasing mass in the form of water, than mass being added to the surface by vesicle adsorption. Hence, spontaneous rupture of single vesicles as well as reaching the critical vesicle coverage at small separated areas on the surface, resulting in patches of SLBs, are possible scenarios occurring before the extrema are reached.[25,26]

The kinetic behavior of the QCM-D signals can be interpreted in greater detail to give information about the properties of the adsorbed vesicles. In particular, the initial slope of the *Df*-plot (the relation between dissipation of the adsorbed layer and added or lost mass) gives an indication of the strength of the initial vesicle-surface interaction. A shallower slope is the result of the adsorption of a molecular layer which is more rigid and hence contributes more to the frequency shift than the dissipation shift. In terms of vesicle adsorption, a shallow slope indicates one of three initial adsorption stages; (i) vesicles that deform as they adsorb to the surface, (ii) vesicles that rupture spontaneously upon adsorption, resulting in SLB patches which contribute minimally to the dissipation shift, or (iii) a combination of both deformed vesicles and SLB patches adsorbed at the surface. Common for the above-mentioned initial adsorption stages is that a shallow initial slope in the *Df*-plot indicates strong vesicle-surface interactions, leading to flattened vesicles and/or the spontaneous formation of SLB patches, which further facilitates vesicle rupture and the formation of a confluent SLB. As can be seen in Figure 1B there is a clear trend with increasing initial slope as the proportion of POEPC is decreased, indicating that the vesicles are less deformed and/or less spontaneous formation of SLB patches occur. Furthermore, the time point at which the extremum in frequency is reached ($t_{\min}$) increased with decreasing proportions of POEPC, which is likely due to the longer times needed for the increased critical coverage to be reached. The final frequency shifts decreased significantly with increased proportions of POEPC while the final dissipation shifts remained at values which are expected for good quality supported bilayers.

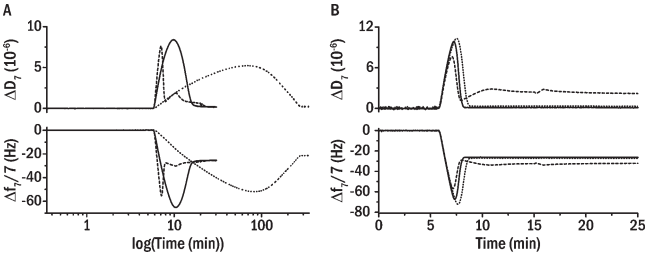

Figure 2. Typical QCM-D responses showing the dissipation and frequency shifts upon the deposition of lipid vesicles composed of POPC (dashed) and POPC doped with 10% (solid) and 20% (dotted) POPS in the presence of (A) 2 mM EDTA and (B) 2 mM calcium ions on flat SiO_2 surface.

(ii) Figure 2 shows the frequency and dissipation shifts during the interaction of vesicles composed of mixtures of the negatively charged lipid POPS and POPC with flat SiO_2 surfaces. At the ratios of POPS studied here, SLB formation was possible despite the negative charge of the support, as can be seen in Figure 2A,B and Table 2. Calcium ions have previously been shown to have a significant effect on vesicle−vesicle[34,35] and in particular on vesicle-surface interactions leading to SLB formation.[25,36] The presence of calcium ions has been demonstrated to decrease the frequency extremum, $\lvert\Delta f_{min}\rvert$,[25] which was explained by an increased vesicle-surface interaction. The same effect was observed here (compare data from POPC SLB formation, i.e. $\lvert\Delta f_{min}\rvert$ = 91.4 ± 14 Hz for 0% POEPC in Table 1 and $\lvert\Delta f_{min}\rvert$ = 85.3 ± 1.4 Hz for 0% POPS with calcium ions in Table 2). Interestingly, a decrease in $\lvert\Delta f_{min}\rvert$ was also observed in the presence of EDTA (see 0% POPS with EDTA in Table 2, $\lvert\Delta f_{min}\rvert$ = 56.7 ± 1.5 Hz) which indicates that EDTA has an effect on the vesicle deposition pathway, in addition to being a calcium chelator.

Increasing the ratio of POPS significantly increased $t_{\min}$, going from minutes to hours, while there were no significant differences in $\lvert\Delta f_{min}\rvert$ (Table 2). This indicates that the intervesicle stress, needed for SLB formation, is similar for the compositions studied here, but that the process takes longer for vesicles with increasing proportions of POPS due to increased vesicle−surface and vesicle−vesicle repulsion. Therefore, the increase in $t_{\min}$, is likely a result of longer times needed for a critical concentration to be reached everywhere at the surface, and the SLB formation propagates more slowly as a result of increased proportions of POPS. The $t_{\min}$ was significantly reduced for compositions with

Table 2. Mean Values and Corresponding Standard Deviations of Parameters Measured by QCM-D upon the Deposition of POPC Vesicles, with Varying Percentages of POPS in the Presence of EDTA or Calcium Ions

POPS (%)	(2 mM)	$\lvert\Delta f_{7,\min}\rvert/7$ (Hz)	$\lvert\Delta D_{7,\max}\rvert$ (10^{-6})	$\Delta f_{7,\text{final}}/7$ (Hz)	$\Delta D_{7,\text{final}}$ (10^{-6})	$t_{\min}$ (min)
0	Ca^{2+}	58.3 ± 1.4	7.84 ± 0.2	−32.4 ± 0.9	2.23 ± 0.3	1.43 ± 0.0
5	Ca^{2+}	70.7 ± 2.9	10.2 ± 0.4	−26.3 ± 0.0	0.19 ± 0.1	1.70 ± 0.1
10	Ca^{2+}	67.4 ± 1.3	9.85 ± 0.3	−26.2 ± 0.2	0.13 ± 0.1	1.53 ± 0.1
20	Ca^{2+}	76.7 ± 5.4	10.9 ± 0.7	−27.2 ± 0.2	0.18 ± 0.1	1.80 ± 0.1
30	Ca^{2+}	71.4 ± 0.9	7.97 ± 0.1	−27.9 ± 0.2	0.19 ± 0.1	3.65 ± 0.3
0	EDTA	56.7 ± 1.5	7.84 ± 0.2	−26.2 ± 0.6	0.40 ± 0.2	1.40 ± 0.0
5	EDTA	66.6 ± 5.2	10.1 ± 0.8	−25.4 ± 0.4	0.10 ± 0.0	1.78 ± 0.1
10	EDTA	69.2 ± 3.0	9.10 ± 0.5	−25.4 ± 0.3	0.12 ± 0.1	4.98 ± 0.4
20	EDTA	54.4 ± 5.2	5.46 ± 0.5	−21.0 ± 3.5	0.28 ± 0.1	102 ± 61

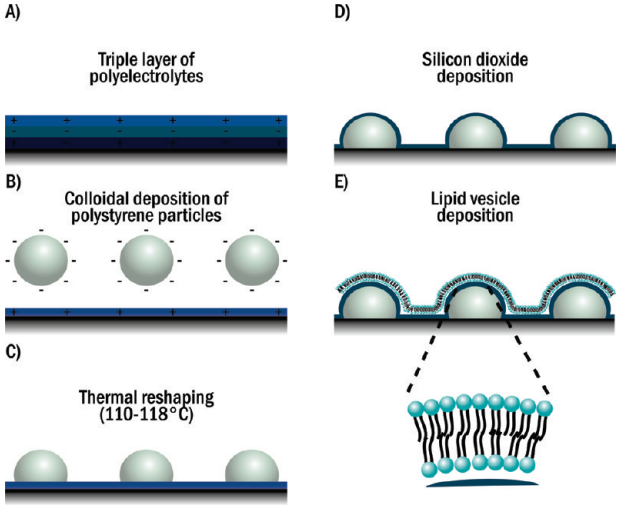

Figure 3. Fabrication of nanostructured substrates for SLB formation via vesicle deposition. (A) deposition of a triple layer followed by (B) colloidal particles. For nanostructures with different ROC thermal reshaping (C) at different temperatures is applied after which (D) the substrates are coated in a layer of silicon dioxide. (E) demonstrates the use of the nanostructured surfaces for templating SLBs with controlled curvature by depositing lipid vesicles that subsequently rupture to an SLB.

10% POPS or higher in the presence of calcium ions compared to EDTA. A likely explanation is the ability of calcium ions to bridge the repulsive charges between the negatively charged vesicles and surface, which would promote vesicle adsorption, deformation, and SLB formation.

As can be seen in Figure 1A (red graph) and Figure 2A (dashed graph) there are additional extrema in the frequency and the dissipation responses respectively for vesicles composed of POPC while they are absent when the SLBs are formed from vesicles containing charged lipids. Additional extrema in both the frequency and dissipation QCM-D responses after the deposition of POPC vesicles and SLB formation have previously been reported on and proposed to be additional vesicles adsorbing to preformed SLB.[15] Here the additional peak is absent when the SLBs are formed from vesicles containing charged lipids, which further supports the theory of vesicles adsorbing to preformed SLB since charged vesicles would exhibit an increased repulsion from the similarly charged preformed SLB.

Fabrication of Nanostructured Surfaces. The nanostructured surfaces are fabricated by colloidal lithography, for an illustration of the fabrication procedure see Figure 3. Figure 4 shows typical SEM images of the nanostructured surfaces. The top row images show the distribution of the heat-treated particles at the surfaces after coating in a SiO_2 layer. There is a shorter wall to wall particle distance as the particles are heated at progressively higher temperatures, while the center to center distances stay the same. The bottom images show the nanostructured surfaces from the side where a clear increase in the convex ROC of the nanostructures can be observed with increased heating temperatures; average ROCs were measured to be 70.4 ± 2.5, 75.1 ± 1.9, and 94.7 ± 4.0 nm for particles heated at 110, 114, and 118 °C, respectively. Figure 5 shows the radial distribution function $g(r)$, which is the concentration of particle centers at a distance r from one particle center normalized to the overall surface concentration of particles, for a monolayer film of 110 nm

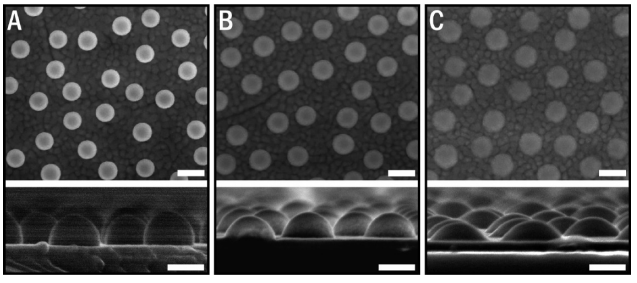

Figure 4. Top view (top row) and side view (bottom row) SEM images of the nanostructured surfaces coated in a silicon dioxide layer with ROCs of (A) 70 nm (heated at 110 °C), (B) 75 nm (heated at 114 °C), and (C) 95 nm (heated at 118 °C). Scale bars are 200 nm for the top row images and 100 nm for the bottom row images.

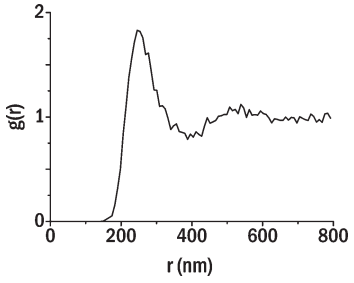

Figure 5. Radial distribution function, $g(r)$, for negatively charged polystyrene colloids (110 nm) adsorbed on silicon dioxide.

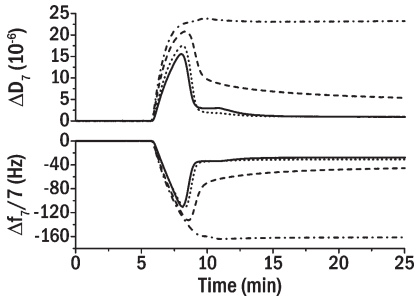

Figure 6. Typical QCM-D responses upon the deposition of POPC vesicles at surfaces with different ROCs: flat (solid), 95 nm (dotted), 75 nm (dashed), and 70 nm (dash-dotted). Vesicle injection at 6 min and a buffer rinse was performed at 10 min.

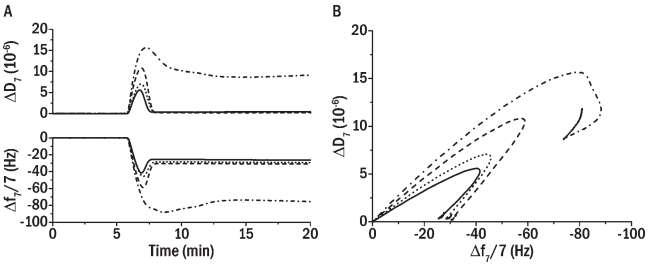

Figure 7. (A) QCM-D responses upon the deposition of 20% POEPC vesicles on surfaces with different ROC: flat (solid), 95 nm (dotted), 75 nm (dashed), and 70 nm (dash-dotted). Vesicle injection at 6 min and buffer rinse at 10 min. (B) Same as part A but plotted as a *Df*-plot.

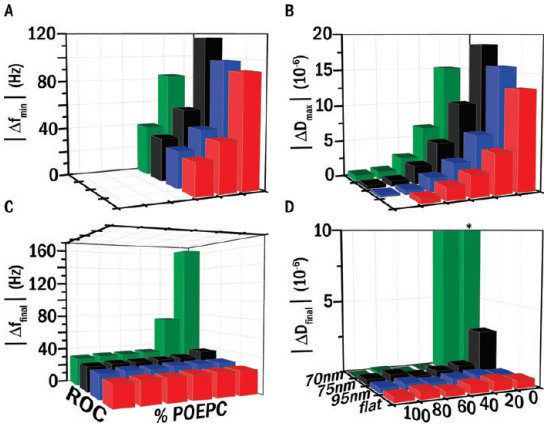

Figure 8. QCM-D results obtained while monitoring POPC vesicles, with systematically increased proportions of POEPC (0, 20, 40, 60, 80, and 100%), interacting with differently curved SiO_2 surfaces (70 nm/green, 75 nm/black, 95 nm/blue, and flat/red). The data presented, (A) minimum frequency shifts, (B) maximum dissipation shifts, (C) final frequency shifts, and (D) final dissipation shifts, are average values from four measurements. For sake of clarity the star (∗) indicates dissipation values that extend beyond the axis of the bar graph ($D = 23 \times 10^{-6}$). The QCM-D responses of the seventh overtone have been normalized to the fundamental frequency.

polystyrene colloids. The primary peak in the radial distribution function indicates the average center-to-center distance between neighboring particles. The peak position is at 250 ± 120 nm (±indicates full width at half-maximum) which is in good agreement with what has previously been shown for similarly sized particle patterns.[31]

Vesicle Adsorption and SLB Formation at Nanostructured Surfaces. The first experiments with vesicle adsorption to nanostructured surfaces were performed with POPC vesicles. The deposition of POPC vesicles at surfaces with convex nanostructures of three different ROCs (70, 75, and 95 nm) can be seen in Figure 6, including as well a flat SiO_2 surface as a reference. The flat surface is considered to have an infinite ROC and as such is discussed as the surface with the largest ROC. The surface with the smallest ROC (70 nm) hindered SLB formation, and vesicles did not rupture, as can be seen from the large dissipation shift and the absence of a minimum in the frequency shift even a long time after adsorption. At surfaces where a substantial amount of SLB was formed (flat and 95 and 75 nm ROC surfaces) the process required a critical coverage of vesicles at the surface for the rupture process to start, as can be seen by the presence of extrema in both the dissipation and frequency shifts (Figure 6). High quality SLBs were formed at the flat surface and at the 95 nm ROC surface. At the 75 nm ROC surface the presence of extrema in both the dissipation and frequency shifts indicate the formation of substantial amounts of SLB but the high final dissipation shift also indicates the presence of intact vesicles at the surface. Final average frequency and dissipation shifts observed were 26.5 ± 0.7 Hz and 0.53 ± 0.3 × 10^{-6} at flat surfaces, 29.3 ± 1.1 Hz and 0.40 ± 0.4 × 10^{-6} at 95 nm ROC surfaces, 37.2 ± 2.7 Hz and 2.91 ± 1.1 × 10^{-6} at 75 nm ROC surfaces, and 163 ± 1.2 Hz and 23.2 ± 0.2 × 10^{-6} at 70 nm ROC surfaces, respectively.

Influence of Positively Charged Lipids. As was shown here and previously,[25] SLB formation via vesicle rupture at flat silicon oxide surfaces is facilitated by the presence of positively charged lipids in the lipid vesicles. Hence, vesicles composed of a mixture of POPC and a fraction of positively charged lipids were deposited at the nanostructured surfaces to induce SLB formation. Figure 7A shows the QCM-D responses upon the deposition of vesicles containing 20% POEPC, and it can be seen how the SLB formation process is facilitated on the smaller ROC surfaces (70 and 75 nm ROC). The absolute final dissipation and frequency shifts at the 75 and 70 nm ROC surfaces (Figure 7A) have decreased significantly compared to what was observed with POPC vesicles (Figure 6), and especially the low dissipation shift observed at the 75 nm ROC surface with vesicles composed of 20% POEPC indicates the formation of an SLB. Average final frequency and dissipation shifts were 26.7 ± 0.4 Hz and 0.65 ± 0.1 × 10^{-6} at flat surfaces, 29.5 ± 0.5 Hz and 0.51 ± 0.1 × 10^{-6} at 95 nm ROC surfaces, 31.4 ± 0.3 Hz and 0.66 ± 0.1 × 10^{-6} at 75 nm ROC surfaces, and 74.7 ± 8.2 Hz and 9.93 ± 1.2 × 10^{-6} at 70 nm ROC surfaces. In the *Df*-plots shown in Figure 7B it can be seen that the initial slope increases with decreased surface ROC, thus pointing toward less deformed vesicles and/or less spontaneous formation of SLB patches on the surfaces with lower ROC.

A systematic study with increased proportions of POEPC was performed to further improve on the final properties of the SLB and the results can be seen in Figure 8, where the average values for the extrema and the final values for the dissipation and frequency shifts are represented. As can be seen in Figure 8A,B, the introduction of the positively charged lipid POEPC resulted in a decrease in $|\Delta f_{min}|$ at each type of surface and the decrease followed the systematic increase in the proportion of POEPC. For vesicles composed of more than 40% POEPC the vesicle

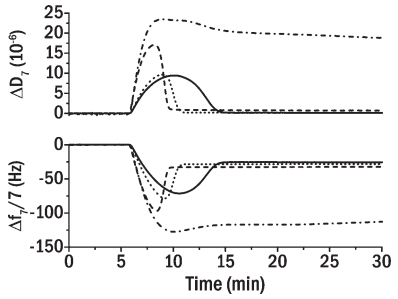

Figure 9. QCM-D responses from the deposition of POPC vesicles doped with 10% POPS in the presence of EDTA on surfaces with different ROC: flat (solid), 95 nm (dotted), 75 nm (dashed), and 70 nm (dash-dotted). Vesicles are injected at 6 min, the pump was stopped at 10 min and started again at 20 min with a buffer rinse.

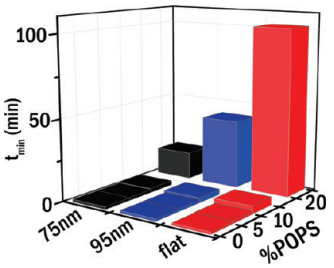

Figure 10. Time point for the minima in the QCM-D frequency response upon the deposition of POPC vesicles doped with 0−20% POPS in the presence of 2 mM EDTA on nanostructured surfaces with different ROCs: flat (red), 95 nm (blue), and 75 nm (black).

deposition pathway no longer resulted in a $|\Delta f_{min}|$ at each type of surface while $|\Delta D_{max}|$ still was present. Similar to what was seen at the flat surface, the final frequency shifts decreased with increased proportions of POEPC for each type of surface (Figure 8C). In addition, for SLB forming compositions, i.e. measurements with low final dissipation shifts, the final frequency shift increased with decreased ROC of the nanostructures. The final dissipation shifts (Figure 8D) were low (within the range of what is expected for supported bilayers) for all curvatures at high proportions of POEPC. When the proportion of POEPC was decreased to 40% or below, the dissipation shifts increased significantly at the 70 nm ROC surfaces as well as for pure POPC at the 75 nm ROC surfaces, indicating the presence of a mixture of SLBs and supported vesicle layers.

Influence of Negatively Charged Lipids. A systematic study with vesicles composed of POPC and a fraction of the negatively charged lipid POPS showed a vesicle deposition process which required a critical coverage of vesicles on the surface for the rupture process to start. The time to reach the critical coverage, i.e., t_{min}, depended on the type of surface as well as on the fraction of POPS in the vesicles. Interestingly, for smaller ROCs, the time to reach the critical coverage, t_{min}, decreased at high POPS ratios. Representative QCM-D responses are shown in Figure 9 with POPC vesicles containing 10% POPS, deposited in the absence of Ca^{2+}. Averaged final frequency and dissipation shifts for vesicles containing 10% POPS in the absence of Ca^{2+} were 25.4 ± 0.3 Hz and 0.12 ± 0.1 × 10^{-6} at flat surfaces, 28.1 ± 0.3 Hz and 0.09 ± 0.1 × 10^{-6} at 95 nm ROC surfaces, 31.9 ± 0.6 Hz and 0.71 ± 0.1 × 10^{-6} at 75 nm ROC surfaces, and 109 ± 5.0 Hz and 18.1 ± 1.1 × 10^{-6} at 70 nm ROC surfaces, respectively. No significant differences in $|\Delta f_{min}|$ and $|\Delta D_{max}|$ for one specific curvature, with varied percentages of POPS, were observed (data not shown). As can be seen in Figure 9, t_{min} is later in time at surfaces with nanostructures of increased ROCs even though the amplitudes of $|\Delta f_{min}|$ are not larger, indicating slower adsorption of negatively charged vesicles at surfaces with increased ROCs. The systematic study of the influence of surface curvature and vesicle charge with respect to t_{min} is summarized in Figure 10. The 70 nm ROC surface is not included, since no SLB formation and hence no t_{min} was observed at that surface. At low proportions of POPS the t_{min} was lowest at the flat surface and increased at surfaces with nanostructures of decreased ROC. Interestingly, for the composition with 10% POPS this trend was reversed and t_{min} was significantly lower at the 75 nm ROC surface and highest at the flat surface; 2.63 ± 0.04 min at 75 nm ROC surfaces, 3.42 ± 0.09 min at 95 nm ROC surfaces, and 4.98 ± 0.40 min at flat surfaces. This trend was even more pronounced for measurements performed with vesicles doped with 20% POPS; 17 ± 2.5 min at 75 nm ROC surfaces, 41.9 ± 30 min at 95 nm ROC surfaces, and 102 ± 61 min at flat surfaces. Even though the average t_{min} values for vesicles with a proportion of POPS of 20% are not significantly different and variation in the data was large, qualitatively the same trend was observed for each individual measurement (where the four different substrates were run in parallel) with longer vesicle adsorption times always observed at surfaces with increased ROC.

As previously mentioned, the presence of the divalent cation Ca^{2+} has a profound effect on the vesicle deposition pathway and hence, Ca^{2+} is commonly used to promote vesicle rupture at flat surfaces.[25,36] Here, whether calcium ions were absent (i.e., no Ca^{2+} was added to the buffer and in addition, EDTA was added to remove residuals of divalent cations) or present during vesicle deposition had a profound effect on vesicle adsorption rates. If calcium ions were present, a significantly shorter t_{min} was observed for all surfaces. The ratio of POPS at which the onset of SLB formation was faster at the nanostructured surfaces compared to the flat was moved to higher proportions of POPS (30% POPS). Similar to the measurements done in the absence of Ca^{2+} in the solutions, the general trend seen when the proportions of POPS was increased in the presence of Ca^{2+} was an increase in t_{min} for each curvature.

Complementary Data by Fluorescence Microscopy. Fluorescence microscopy was utilized as a complementary tool to the QCM-D technique to study the properties of the deposited lipids at the differently curved surfaces. The findings from the QCM-D measurements were supported by the data taken by fluorescence microscopy. Representative images of SLBs formed from the compositions POEPC and 10% POPS in the absence and presence of calcium ions are shown in Figure 11, parts A, B, and C (top row) respectively. The SLBs have been formed at SiO_2 coated substrates patterned with nanostructures (95 nm ROC) on the top half and no nanostructures (flat) on the bottom half. The total fluorescence intensities, for all compositions, were significantly higher at the nanostructured half of the wafers compared to the flat, indicating increased amounts of lipids at the nanostructured half. This trend of increasing fluorescence intensities on the nanostructured part of the substrates was seen for all curvatures. The total fluorescence intensity increased with decreased ROC and the ratio between the nanostructured half and the flat half was 1.3−1.4 at the 95 nm ROC surface, 1.4−1.5 at the 75 nm ROC surface, and ~1.5 at the 70 nm ROC surface. FRAP measurements on the three different compositions at

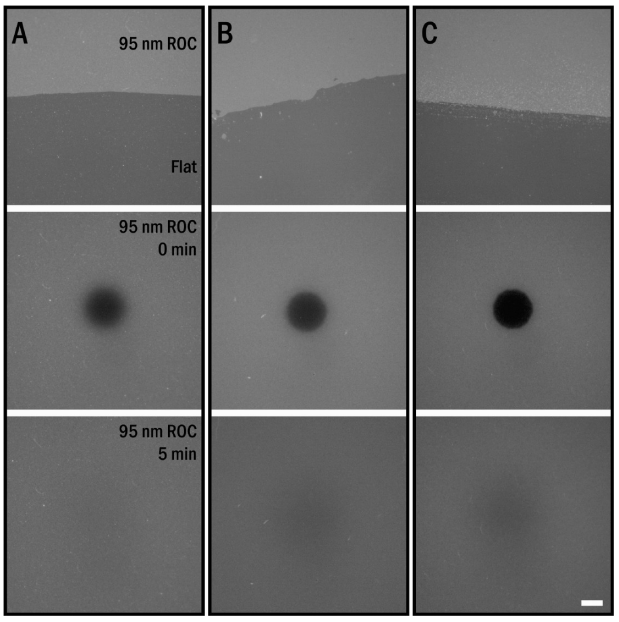

Figure 11. Fluorescence microscopy images of SLBs formed from vesicles composed of (A) POEPC, and binary mixtures of POPC and (B) 10% POPS in the presence of EDTA, and (C) 10% POPS in the presence of calcium ions. At the top row, SLBs have been formed at stripped wafers with the top half containing SiO_2-coated nanoparticles with 95 nm ROCs and the bottom half containing flat SiO_2. FRAP measurements performed at nanostructured surface with 95 nm ROC are shown in the middle (images taken directly after bleaching) and bottom rows (images taken 5 min after bleaching). The scale bar is 20 μm.

95 nm ROC surfaces are shown in Figure 11, parts A, B, and C (middle and bottom row). The middle row images were taken directly after bleaching a small spot of the SLBs and the bottom row images were taken 5 min after bleaching and show almost total recovery of the bleached spot. FRAP on surfaces exposed to vesicles composed of POEPC showed full recovery at all different ROC surfaces, supporting the QCM-D data of the formation of SLBs. Nanostructured surfaces with a ROC of 70 nm exposed to vesicles composed of 10% POPS did not show recovery which indicates the presence of an immobile vesicle layer adsorbed at the surface.

DISCUSSION

First, possible mechanisms for vesicle adsorption and subsequent SLB formation, for the differently curved nanostructured surfaces, are presented. Second, the influence of the incorporation of the positively charged lipid POEPC or the negatively charged lipid POPS, in vesicles composed of zwitterionic lipids, on SLB formation is discussed. This is followed by a discussion on the effect of nanostructures in interfering with the formation of SLBs and finally, the level to which the SLBs conform to the underlying nanostructures is elaborated upon.

Mechanisms for Vesicle Adsorption and SLB Formation. The vesicle adsorption process was shown to be dependent on vesicle charge for negatively charged vesicles, with significantly lower adsorption rates observed for high contents of negatively charged lipids in the vesicles. Little or no influence of vesicle charge, on vesicle adsorption, was observed for positively charged vesicles. On the basis of these observations two models are

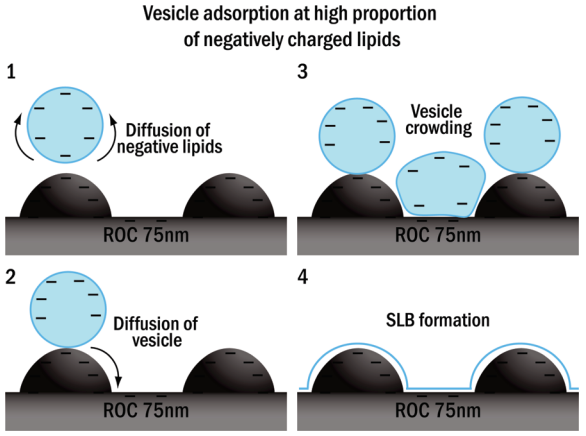

Figure 12. Schematic representation of a potential mechanism for the adsorption of highly negatively charged vesicles to convex nanostructured surfaces, with nanostructures on a size scale which is similar to that of the vesicles.

presented: model 1, which is valid for highly negatively charged vesicles, and model 2, which is valid for positively, neutral, and low negatively charged vesicles. Note that general mechanisms for positively and negatively charged vesicles are proposed, but differences in the adsorption and SLB formation routes, due to specific properties of the lipids, can occur.

(1) For negatively charged vesicles, the adsorption rates decreased with increasing proportions of negatively charged lipids, as expected based on the increased repulsion between the negatively charged surface and the negatively charged vesicles in the bulk.[25] Interestingly, the adsorption rate was the highest at the flat surface and decreased with decreased ROC at low ratios of POPS, a trend which was reversed at high ratios of POPS and the lowest adsorption rate was observed at the flat surface. In addition, the same trend with decreasing adsorption rates with increasing proportions of POPS was also observed in the presence of calcium ions, but then with an onset at higher proportions of negatively charged lipids. These data indicates (i) that it is mainly the negatively charged lipids that contribute to the repulsion, as opposed to negatively charged EDTA molecules possibly intercalated in the lipid membrane and (ii) that the presence of nanostructures reduces the effect of the repulsion between the surface and the negatively charged vesicles in the bulk. In addition, the lower the ROC of the structures the more significant was the reduction in repulsion. One potential mechanism is that at high POPS ratios, the topographic structures provide sites for vesicle adsorption (see illustration in Figure 12). The convex shape of the nanostructures would provide a lower initial surface area with an interacting spherical vesicle and a longer geometric distance between the surface and the lipid vesicle, in the region around the contact area, compared to a flat surface. The repulsion from the negatively charged surface, as felt by the negatively charged vesicles, will therefore be narrowed to a smaller effective area. Furthermore, it is possible that the presumably initially homogeneously distributed lipids redistribute within each leaflet, such that the negatively charged lipids diffuse away from the section of the vesicle which is facing the negatively charged

dx.doi.org/10.1021/jp2025363 |J. Phys. Chem. B 2011, 115, 7838–7848

surface, and toward the top of the vesicles. Less redistribution can be expected to be needed for vesicles adsorbing at the convex structures where the contact area is smaller compared to a flat surface. As a consequence, the adsorption rate is expected to be higher the lower the ROC, which is observed in the QCM-D experiments. It should be noted that such an adsorption mechanism would concomitantly result in a reduced adsorption rate at the flat sites close to and between the nanostructures, due to the increased repulsion from the nanoparticle walls. At surfaces with nanoparticles of decreased ROCs, not only adsorption rates but also the SLB formation process as a whole is faster (as seen by QCM-D) for elevated percentages of negatively charged lipids. As a consequence, the vesicles adsorbing at an increased rate on the nanostructures must also be contributing to the vesicle crowding in order to affect the SLB formation rate. That this should occur does not obviously follow from an increased adsorption rate at the nanostructures since surfaces with nanostructures have a higher total surface area. If vesicles move from the top of the convex nanostructures to the flat part of the surface, additional vesicles would be able to adsorb (at a fast rate) to the apex of the nanostructures, and the surface will be filled up with vesicles faster than on a flat surface. There are reports in the literature that argue against[25] as well as for[37] vesicle movement on flat surfaces. However, the movement required for this mechanism to be true is only on the order of some tens of nanometers. In addition, movement of vesicles may well be enabled by a surface with curvatures that change from convex to concave across the size scale of a single vesicle. An alternative explanation for the shorter times to reach the critical coverage may be that the crowding occurs exclusively on the convex parts of the surface, and that SLB formed by intervesicle induced rupture on the nanostructures promote vesicle adhesion and rupture at the flat parts. This theory does not require vesicle mobility on the surface but what speaks against it is that only little crowding may be possible or the crowding is less efficient on the nanostructures. Because of the convex shape of the nanostructures it is possible that the stress felt by neighboring vesicles is reduced and hence making vesicle rupture less likely.[38]

(2) At low proportions of negatively charged lipids and with vesicles composed of neutral or positively charged lipids there is no increased benefit of vesicles adsorbing to the convex nanostructures. Theoretical investigations have shown that adsorption of vesicles to structures of similar sizes as the vesicles require higher contact potentials at structures with convex shapes compared to concave shapes.[39] As a consequence, it is more likely that vesicle adsorption is promoted close to and between the nanostructures to a higher extent than at the apex of the nanostructures. SLB formation is then mainly expected to occur, at a critical coverage of vesicles, at the flat parts. The formation of bilayer edges could further promote vesicle adsorption and rupture at the convex parts (also true for mechanism 1). Adsorption of highly positively charged vesicles is expected to be more or less equal all over the surface due to the strong vesicle-surface interaction, a theory supported by the spontaneous formation of SLBs (or by a need for only small amounts of intervesicle stress) as observed by QCM-D.

Influence of Vesicle Charge on SLB Formation. Similar to what has previously been shown using the lipids DOPC, DOTAP, and DOPS[25] the vesicle deposition pathway can be tuned by varying the net charge of the lipid vesicle by utilizing the lipids POPC, POEPC, and POPS. The inclusion of the positively charged lipid POEPC in zwitterionic lipid vesicles facilitates vesicle rupture, at flat and nanostructured surfaces, which can be explained by the stronger interaction between the positively charged vesicles and the negatively charged surface. As a consequence, for increased proportions of POEPC a decreased stress, in the form of a cooperative action of neighboring vesicles, is required for the vesicle rupture process to start. At 40% POEPC and higher, the extremum in the frequency response was absent, indicating spontaneous rupture or only the need for little crowding for the rupture process to start. At TiO_2 surfaces, pure POEPC vesicles have been shown to form SLBs through a process needing neighboring vesicles,[40] which stresses the importance of the properties of the solid support for the vesicle deposition pathway. The final frequency shifts decreased with increased proportions of POEPC, a trend which has been shown before for DOTAP and DOPC.[25] A likely explanation is increased repulsion between the positively charged lipid head groups resulting in a less dense supported bilayer. Alternatively, a smaller frequency shift could be a result of increased defects in the membrane. Fluorescence microscopy data, however, suggest that no such defects are present.

As expected, the presence of negatively charged lipids in the lipid vesicles made the process of forming SLBs more difficult, explained by the decreased interaction between the vesicles and the surface. This could, to some extent, be overcome by introducing the divalent cation Ca^{2+} in the buffer which can bridge the negative vesicle and surface charges. Interestingly, the presence of EDTA in the buffer also had an effect on the vesicle deposition pathway; i.e., the critical coverage was reduced. It has previously been shown that EDTA destabilizes lipid membranes by intercalating within the lipid membrane.[41] Such a membrane destabilization could explain the decreased extrema in the frequency shifts observed here in the presence of EDTA.

Nanostructured Stabilization of Vesicles. Findings presented here indicated that the supported bilayers formed were in general of higher quality at flatter surfaces and the quality decreased with decreasing convex ROCs. The structures have at least two ROCs. In addition to the convex ROC, there is also a concave ROC at the contact point between the nanostructure and the flat surface. From the SEM images (Figure 4) it can be seen that the ROCs in these regions are small and since they are situated at the base of the adsorbed particles, they are expected to contribute little to the event of adsorption and rupture of lipid vesicles. During vesicle adsorption and rupture, the convex parts, both on the top and the side of the structures, are expected to have the biggest influence (see below). We have thus correlated the behavior of the lipid vesicles to the magnitude of the convex ROC. However, for the discussion of a confluent SLB to the nanostructured surface, the concave parts are also expected to play a role, which will be discussed further below.

The presence of extrema in the frequency shifts, for almost all compositions and surfaces, suggests that the vesicle-surface interactions are not enough to induce immediate spontaneous vesicle rupture. The extrema in the dissipation and frequency shifts indicate that additional stress, in the form of neighboring vesicles, is required for SLBs to form.[24] The presence of convex nanostructures, of similar sizes as the adsorbed lipid vesicles, was

Table 3. Correlation between Increased Surface Area, Due to the Presence of Nanostructures, and Increased Frequency Shifts, As Measured by QCM-D

ROC	70 nm	75 nm	95 nm
A_{nano}/A_{flat}	1.34	1.23	1.13
$f_{POEPC,\ nano}/f_{flat}$	1.32[a]	1.16[a]	1.10[a]
$f_{POPS+EDTA,\ nano}/f_{flat}$	4.75[b]	1.21[a]	1.10[a]
$f_{POPS+Ca,\ nano}/f_{flat}$	5.35[b]	1.55[c]	1.12[a]

[a] SLB forming composition. [b] Supported vesicle layer. [c] Partly forming SLB.

shown to further hinder SLB formation. Similar results have previously been shown by Weng et al.[38] where lipid vesicles were deposited at xerogels with silica grains and pores of the same dimensions as the vesicles and the SLB formation process was slowed down. In our study, *Df*-plots (Figure 7B) imply that vesicles are more deformed, i.e., flatter, and/or the spontaneous formation of SLB patches increases at surfaces with increased ROCs. These data suggest that vesicles at a flat surface are free to deform, and the degree of deformation is mainly balanced by the vesicle−surface interactions (leading to vesicle deformation) and the membrane bending energy (resisting vesicle deformation). Vesicles adsorbed at the nanostructured surfaces show a steeper initial *Df*-gradient, which indicates that the nanostructures stabilize the vesicles, most likely by interactions of the vesicles with the walls of the nanostructures. Further support for this theory is gained from the increasingly steeper gradients of the *Df*-plots observed for decreasing ROCs (increasing curvature), which would be expected if the vesicles were stabilized between the progressively taller structures. Such stabilization of vesicles at nanostructured surfaces would result in the vesicles not being able to deform to the same extent as on a flat surface, and as a consequence there could be a need for increased intervesicular stress in order to form SLBs. In addition, less efficient crowding, as previously proposed by Weng et al.,[38] due to the vesicles being adsorbed unevenly in height, could result in the need for increased critical coverage before the rupture process starts. In the data presented here there is a trend of increasing $|\Delta f_{min}|$ with decreasing ROCs (Figure 7A and 8A) which could indicate the need for increased critical coverage with decreasing ROC but the interpretation is complicated by the increased total surface area generated by nanostructures of decreasing ROC which contributes to an increase in $|\Delta f_{min}|$.

Conformal SLBs. Conformal supported bilayers, formed by vesicle rupture, on nanostructured silica surfaces of similar curvatures as those used here have previously been confirmed by Roiter et al.[10] They show that for a particle radius of 0.6−11 nm the bending energy of the lipid bilayer conforming to the particle exceeds the adhesion energy and the SLB forms a pore around the particle, while a particle radius >11 nm resulted in conformal SLBs. In agreement with these results, findings presented here indicate that the supported membranes conform to the underlying nanostructures based on the significant increase in mass (measured by the QCM) observed at surfaces with nanostructures of decreased ROCs (see Table 3). In Table 3 the correlation between increased surface area, provided by the presence of nanostructures of different curvatures, and increased mass deposited at the surface, as measured by QCM-D, is presented. From Table 3 it can be seen that the increased mass scales well with the increased surface area provided by the nanostructures.

It was previously argued that the concave parts of the surface played a minor role in vesicle adsorption and rupture. However, when comparing the increase in total surface area, due to the presence of nanostructures, with that of the expected mass on the surface in the form of a SLB, the concave ROCs are expected to play a role. Because of the increased bending energy in the lipid membrane at areas with small concave ROCs, the lipid membrane may not perfectly follow the curvatures. As a consequence, this would result in less mass in the form of SLB at the surface than expected and more mass, in the form of trapped water between the SLB and the concave parts of the surface, as detected by the QCM-D, which might cancel each other out.

Conformal membranes are further supported by fluorescence microscopy measurements. The total fluorescence intensities, for SLB forming compositions, are significantly higher at the parts of the wafers that contain nanostructures compared to the flat parts. In addition, the increase in total fluorescence was bigger for surfaces with decreased ROC, i.e. at surfaces with increased surface area. FRAP measurements confirmed fluid supported membranes as opposed to supported (immobile) vesicles. Together, these data suggest that conformal fluid supported membranes are formed at the nanostructured surfaces.

CONCLUSIONS

In conclusion, it was shown that SLBs could be formed from a wide range of charged vesicles at interfaces with controlled curvatures. Conformal SLBs were confirmed from corroborating QCM-D and fluorescence microscopy data. An increase in lipid mass, indicated by both increased frequency responses and total fluorescence intensities, was shown at surfaces with decreased ROCs, i.e. increased surface area. The presence of convex nanostructures of decreasing ROCs made it progressively harder to form good quality supported bilayers, likely due to vesicle stabilization by the walls of the nanostructures. At high enough proportions of positively charged lipids, it was possible to form good quality SLBs at all curvatures studied: flat and 70, 75, and 95 nm ROC. This could be explained by the increased vesicle-surface interactions resulting in membrane stress by vesicle deformation. When introducing negatively charged lipids, the adsorption rates were significantly reduced, an effect that was more pronounced on surfaces with decreased curvatures. In the presence of calcium ions, adsorption rates for negatively charged vesicles were increased, which was explained by the charge shielding property of calcium ions. The presence of negatively charged lipids hindered SLB formation and increasing proportions of POPS in the vesicles decreased the SLB quality. Vesicles composed of increasing proportions of negatively charged lipids required surfaces with nanostructures of progressively increasing ROCs for the formation of good quality SLBs. From these data a mechanism for vesicle adsorption and subsequent rupture was presented. It is proposed that vesicle adsorption, at high POPS proportions, is promoted at the convex nanoparticles due to the decreased vesicle-surface electrostatic repulsion. Vesicle diffusion from the particle apex to the flat parts of the surface allows for vesicle crowding and SLB formation. For vesicles that are only slightly negatively charged, neutral, or positively charged, surface adsorption is likely promoted at the flat parts between the nanoparticles, justified by the possibilities of increased vesicle-surface interactions with the walls of the nanostructures. The lipid membranes formed here, with both different lipid

compositions and ROCs, should be applicable to a range of studies of cell membrane related processes such as curvature induced lipid sorting and protein binding.

AUTHOR INFORMATION

Corresponding Author

*E-mail: duncan@inano.au.dk. Telephone: +45 8942 5547. Fax: +45 8942 3690.

ACKNOWLEDGMENT

This work was funded by the Danish Research Council (Internationalization grant 1-5971-10000256). We thank Jacques Chevallier (University of Aarhus) for help with sample preparation and Hans P. Jakobsen for providing the program for calculating the radial distribution function.

REFERENCES

(1) Sheetz, M. P. *Nat. Rev. Mol. Cell Biol.* **2001**, *2*, 392–396.
(2) Marsh, M.; McMahon, H. T. *Science* **1999**, *285*, 215–220.
(3) Scott, I. C.; Stainier, D. Y. R. *Nature* **2003**, *425*, 461.
(4) Bacia, K.; Schwille, P.; Kurzchalia, T. *Proc. Natl. Acad. Sci. U.S.A.* **2005**, *102*, 3272–3277.
(5) Roux, A.; Cuvelier, D.; Nassoy, P.; Prost, J.; Bassereau, P.; Goud, B. *EMBO J.* **2005**, *24*, 1537–1545.
(6) Hatzakis, N. S.; Bhatia, V. K.; Larsen, J.; Madsen, K. L.; Bolinger, P. Y.; Kunding, A. H.; Castillo, J.; Gether, U.; Hedegard, P.; Stamou, D. *Nat. Chem. Biol.* **2009**, *5*, 835–841.
(7) Werner, J. H.; Montano, G. A.; Garcia, A. L.; Zurek, N. A.; Akhadov, E. A.; Lopez, G. P.; Shreve, A. P. *Langmuir* **2009**, *25*, 2986–2993.
(8) Parthasarathy, R.; Yu, C. H.; Groves, J. T. *Langmuir* **2006**, *22*, 5095–5099.
(9) Jonsson, M. P.; Jonsson, P.; Hook, F. *Anal. Chem.* **2008**, *80*, 7988–7995.
(10) Roiter, Y.; Ornatska, M.; Rammohan, A. R.; Balakrishnan, J.; Heine, D. R.; Minko, S. *Nano Lett.* **2008**, *8*, 941–944.
(11) Brian, A. A.; McConnell, H. M. *Proc. Natl. Acad. Sci. U.S.A.* **1984**, *81*, 6159–6163.
(12) Reimhult, E.; Hook, F.; Kasemo, B. *J. Chem. Phys.* **2002**, *117*, 7401–7404.
(13) Claesson, M.; Cho, N. J.; Frank, C. W.; Andersson, M. *Langmuir* **2010**, *26*, 16630–16633.
(14) Pfeiffer, I.; Petronis, S.; Koper, I.; Kasemo, B.; Zach, M. *J. Phys. Chem. B* **2010**, *114*, 4623–4631.
(15) Sundh, M.; Svedhem, S.; Sutherland, D. S. *Phys. Chem. Chem. Phys.* **2010**, *12*, 453–460.
(16) Richter, R. P.; Berat, R.; Brisson, A. R. *Langmuir* **2006**, *22*, 3497–3505.
(17) Seantier, B.; Breffa, C.; Felix, O.; Decher, G. *J. Phys. Chem. B* **2005**, *109*, 21755–21765.
(18) Reimhult, E.; Hook, F.; Kasemo, B. *Phys. Rev. E* **2002**, *66*.
(19) Reimhult, E.; Hook, F.; Kasemo, B. *Langmuir* **2003**, *19*, 1681–1691.
(20) Justesen, P. H.; Kristensen, T.; Ebdrup, T.; Otzen, D. *J. Colloid Interface Sci.* **2004**, *279*, 399–409.
(21) Zimmerberg, J.; Kozlov, M. M. *Nat. Rev. Mol. Cell Biol.* **2006**, *7*, 9–19.
(22) Rao, N. M. *Chem. Phys. Lipids* **2010**, *163*, 245–252.
(23) Bonifacino, J. S.; Lippincott-Schwartz, J. *Nat. Rev. Mol. Cell Biol.* **2003**, *4*, 409–414.
(24) Keller, C. A.; Kasemo, B. *Biophys. J.* **1998**, *75*, 1397–1402.
(25) Richter, R.; Mukhopadhyay, A.; Brisson, A. *Biophys. J.* **2003**, *85*, 3035–3047.
(26) Reviakine, I.; Brisson, A. *Langmuir* **2000**, *16*, 1806–1815.
(27) Richter, R. P.; Maury, N.; Brisson, A. R. *Langmuir* **2005**, *21*, 299–304.
(28) Rossetti, F. F.; Textor, M.; Reviakine, I. *Langmuir* **2006**, *22*, 3467–3473.
(29) Merz, C.; Knoll, W.; Textor, M.; Reimhult, E. *Biointerphases* **2008**, *3*, FA41–FA50.
(30) Kunze, A.; Svedhem, S.; Kasemo, B. *Langmuir* **2009**, *25*, 5146–5158.
(31) Hanarp, P.; Sutherland, D. S.; Gold, J.; Kasemo, B. *Colloids Surf., A: Physicochem. Eng. Asp.* **2003**, *214*, 23–36.
(32) Andersson, A. S.; Glasmastar, K.; Hanarp, P.; Seantier, B.; Sutherland, D. S. *Nanotechnology* **2007**10.1088/0957-4484/18/20/205303 .
(33) Edvardsson, M.; Svedhem, S.; Wang, G.; Richter, R.; Rodahl, M.; Kasemo, B. *Anal. Chem.* **2009**, *81*, 349–361.
(34) Kachar, B.; Fuller, N.; Rand, R. P. *Biophys. J.* **1986**, *50*, 779–788.
(35) Sinn, C. G.; Antonietti, M.; Dimova, R. *Colloids Surf., A-Physicochem. Eng. Asp.* **2006**, *282*, 410–419.
(36) Rossetti, F. F.; Bally, M.; Michel, R.; Textor, M.; Reviakine, I. *Langmuir* **2005**, *21*, 6443–6450.
(37) Weirich, K. L.; Israelachvili, J. N.; Fygenson, D. K. *Biophys. J.* **2010**, *98*, 85–92.
(38) Weng, K. C.; Stalgren, J. J. R.; Duval, D. J.; Risbud, S. H.; Frank, C. W. *Langmuir* **2004**, *20*, 7232–7239.
(39) Das, S.; Du, Q. *Phys. Rev. E* **2008**, *77*, 011907.
(40) Kunze, A.; Sjovall, P.; Kasemo, B.; Svedhem, S. *J. Am. Chem. Soc.* **2009**, *131*, 2450–2451.
(41) Prachayasittikul, V.; Isarankura-Na-Ayudhya, C.; Tantimongcolwat, T.; Nantasenamat, C.; Galla, H. J. *Acta Biochim. Biophys. Sin.* **2007**, *39*, 901–913.